Particle trajectories by arc spraying with cored wires

W. Tillmann, E. Vogli, M. Abdulgader, M. Gurris, D. Kuzmin, S. Turek, Dortmund/D

To use the manifold possibilities that arc spraying offers to deposit wear resistance layers, the knowledge of the particle formation and their characteristics are necessary. The work is focused on studying the particle trajectories during arc spraying with cored wires. Different cored wires under various spraying parameters are investigated by means of a high speed camera. Particle properties in-flight, such as velocity and temperature are determined. Correlation between particle trajectories and particle characteristics at different spraying conditions are established.
At the same time, the particle-laden gas flow is simulated numerically and the computed solutions are used to illustrate the utility of the proposed CFD model and compared with experimental results. The employed mathematical model represents a system of macroscopic conservation laws for the continuous gas phase and for the gas-solid mixture. This formulation makes it possible to circumvent the numerical difficulties associated with the implementation of a (potentially ill-posed) two-fluid model. The discretization in space is performed using a high-resolution finite element scheme based on algebraic flux correction in terms of local characteristic variables. The artificial diffusion operator is constructed on the discrete level and fitted to the local solution behavior using a multidimensional flux limiter of TVD type.

1 Introduction

The twine wire arc spraying (TWAS) technique is regarded as versatile spraying process, where the materials to be sprayed in wire form are melted [1]. The melted materials are atomized and accelerated towards the substrate by means of pressurized air. Thereby the coatings properties are considered to be a sum of the process parameters, which directly or indirectly influence the particle formation, size, velocity and temperature [2-3]. Lampann [4] found out by spraying metallic wires through TWAS that the particle formation is strongly affected by the atomization gas pressure. By applying low atomization gas pressure (less than 2 bars) are predominantly generated thread-shaped particles. With increase of atomization gas pressure the molten wire materials are directly atomized at the electrode spikes, without flowing out the molten bath. The generated primary particles will further atomize under influence of the high atomization gas pressure and the turbulent stream in so called secondary particles, which are smaller in size than the primary particles. Thereby the particle size distribution exhibits a broad spectrum associated with an inhomogeneous coating morphology. Wen et al. [5], Watanabe et al. [6] and Hussary et al. [7] came to the same conclusion. They stated that a homogenous structure by TWAS process can be generated through fast and small particles at high temperatures.
Recently the use of cored wires has extended the field of TWAS application. The inhomogeneous composition of the cored wires causes an additional uncertainty in particle formation and characteristic features of particles in flight [8-9]. In order to have a good coating quality produced by means of cored wires and to secure the reproducibility of a desired coating an accurate interpretation of the particle formation and particles in flight characteristics is needed.
In addition to process and coatings characterization effort has been made to describe the spraying processes through mathematical models [10-11]. For example, the flow behavior in a plasma torch and plasma flow after powder feeding in a plasma spraying process are described with multi-phase compressible flow models, while the particle broadening and solidification as well as the determination of their size and form are characterized by employing of the incompressible Navier-Stokes equations. Kamnis et al. [12] developed mathematical models to predict particle dynamic behavior in a liquid fuel high velocity oxy-fuel thermal spray gun. They applied a 3-dimensional CFD model, which employed a Lagrangian particle tracking frame coupled with a steady-state gas flow field.
In this work an online diagnostic of particles was utilized to measure their velocity and temperature along the spray jet. The particle sizes were examined through analyzing of sprayed particles, which are quenched in water. In addition to the experimental work a mathematical model was developed and applied to TWAS process. In contrast to [12] the mathematical modeling was based on an Euler/Euler approach. The theoretical and experimental results were compared and aligned for further optimization of the mathematical model.

2 Experimental Set Up

2.1 Mathematical model

Mathematical models of particle-laden gas flows are usually based on macroscopic conservation laws that can be postulated or derived using a suitable averaging procedure [13-17]. Neglecting molecular diffusion and turbulence, one obtains a set of partial differential equations for the mass, momentum, and energy of the continuous gas phase:

$$\partial_t(\alpha_g\rho_g) + \nabla\cdot(\alpha_g\rho_g\bar{u}_g) = 0 \quad (1)$$

$$\partial_t(\alpha_g\rho_g\bar{u}_g) + \nabla\cdot(\alpha_g\rho_g\bar{u}_g\otimes\bar{u}_g + \alpha_g P_g I) = \gamma_D\alpha_p(\bar{u}_p - \bar{u}_g) \quad (2)$$

$$\partial_t(\alpha_g\rho_g E_g) + \nabla\cdot(\alpha_g\bar{u}_g(\rho_g E_g + P_g) = \gamma_D\alpha_p\bar{u}_p(\bar{u}_p - \bar{u}_g) \quad (3)$$

where α_g, ρ_g, $\bar{u}_g$, P_g and E_g are the volume fraction, density, velocity, pressure and total energy of the inviscid gas. The constant coefficient γ_D denotes the rate of interphase momentum transfer due to the viscous drag force [15]. For simplicity, all other forces (virtual mass and lift) as well as mass and heat transfer effects are neglected. A similar system of conservation laws can be formulated for the disperse particle phase (index p):

$$\partial_t(\alpha_p\rho_p) + \nabla\cdot(\alpha_p\rho_p\bar{u}_p) = 0 \quad (4)$$

$$\partial_t(\alpha_p\rho_p\bar{u}_p) + \nabla\cdot(\alpha_p\rho_p\bar{u}_p\otimes\bar{u}_p + \alpha_p P_g I) = \gamma_D\alpha_p(\bar{u}_g - \bar{u}_p) \quad (5)$$

$$\partial_t(\alpha_p\rho_p E_p) + \nabla\cdot(\alpha_p\bar{u}_p(\rho_p E_p + P_g) = \gamma_D\alpha_p\bar{u}_p(\bar{u}_g - \bar{u}_p) \quad (6)$$

It is commonly assumed that the pressure P_g is the same for both phases and satisfies the equation of state:

$$P_g = (\gamma - 1)\rho_g\left(E_g - \frac{|\bar{u}_g|^2}{2}\right) \quad (7)$$

Furthermore, the volume fractions of the continuous and disperse phase are coupled by the constraint:

$$\alpha_g + \alpha_p \equiv 1 \quad (8)$$

Inviscid two-fluid models like (1)–(6) are particularly difficult to solve numerically due to the lack of hyperbolicity and uncertainty regarding the modeling of the disperse phase in particle-free regions. If the volume fraction of particles equals zero, the same behavior show the effective density $\alpha_p\rho_p$ and momentum $\alpha_g\rho_g\bar{u}_g$. As a consequence, the velocity of particles $\bar{u}_p$ is not uniquely defined, which may give rise to nonphysical solutions and waves moving at wrong speeds. Clearly, such a potentially degenerate two-fluid model is of little practical utility. In order to circumvent the above mathematical and numerical difficulties, the gas-particle mixture was considered as a single fluid. The effective density, momentum and energy of the mixture are given by the following equations:

$$\rho = \alpha_p\rho_p + \alpha_g\rho_g \quad (9)$$

$$\rho\bar{u} = \alpha_p\rho_p\bar{u}_p + \alpha_g\rho_g\bar{u}_g \quad (10)$$

$$\rho E = \alpha_p\rho_p E_p + \alpha_g\rho_g E_g \quad (11)$$

The so-defined conservative variables ρ, $\rho\bar{u}$ and ρE are assumed to satisfy the compressible Euler equations:

$$\partial_t(\rho) + \nabla\cdot(\rho\bar{u}) = 0 \quad (12)$$

$$\partial_t(\rho\bar{u}) + \nabla\cdot(\rho\bar{u}\otimes\bar{u} + P_g I) = 0 \quad (13)$$

$$\partial_t(\rho E) + \nabla\cdot(\bar{u}(\rho E + P_g) = 0 \quad (14)$$

By definition of the mixture density ρ the continuity equation (12) is the sum of (1) and (4). The effective pressure of the mixture can also be defined as P_g plus a correction describing the influence of the particles [18-19].

In the present work, we solve equations (12)–(14) instead of (1)–(6), whereby the density, momentum and energy of the particulate phase can be readily inferred from algebraic relations (9)–(111). This formulation can be classified as a drift-flux model. The PDE system to be solved consists of subproblems (1)–(3) and (12)–(14) both of which reduce to the Euler equations of gas dynamics in particle-free regions, where the standard two-fluid model (1)–(6) is not applicable.

2.2 Spraying experiments

To study the particle trajectories by arc spraying an arc spraying device with a closed nozzle system Smart Arc 350 PPG Fa. Sulzer Metco was used. As feedstock a Fe-based and a Ni-based cored wire with a diameter of 1.6 mm were employed (**Tab. 1**).

Tab. 1: Composition of the employed wires.

Wire	Content [Weight %]
FeCrBSiMn	Cr-29; Mn-1,6; Si-1,6; B-3,8; Fe-Bal.
NiCrBSi+PC	Cr-24; Si-5,25; B-1,8; PC-0,4; Ni-Bal.

Aimed to analyze the particles` formation as well as their temperature and velocity along the spray jet the stand-off distance was varied between 45 and 150 mm, while other spraying parameters were kept constant, **Tab. 2**. The electric current and voltage level were taken from prior works, in which the arc ignition stability and arc fluctuations were analyzed [20].

Tab. 2: Arc spraying process parameters.

Parameter	Parameter Value
Current [A]	320
Voltage [V]	32
Primary air pressure [bar]	6
Spraying distance [mm]	45-150

The particle temperature and velocity at different stand-off distances were measured by means of Accuraspray-g3 (Tecnar, Canada). The properties are measured within two measuring volumes with a dimension 3x25 mm. Through a dual fiber optical system the flow of particles at two different points along the spray jet were detected and the velocity is determined as a ratio of the gap between two measuring points and the time delay. Based on the twin wave length pyrometer principle the mean particle temperature is measured. In this case it was been assumed that the emissivity of the particles is the same for the two wave lengths.

The particle formation and atomization were analyzed by means of a high speed camera (PCO, Germany). This camera system comprises an image splitter unit, four intensified CCD camera modules with fast switchable MCP image intensifiers and high resolution CCD image sensors. Each module with its 12 bit dynamic range and a high resolution CCD image sensor features a really good signal-to-noise-ratio and the ability of single photon detection. Four high speed serial fiber optic data links connect the system to the PC. To investigate the particle size during arc spraying experiments a custom-made experimental set-up was designed and applied (for more details see [20]). The generated particles were analyzed by means of light microscopy (Zeiss, Germany) and SEM (SEM, JSM-840, Co. Jeol, Japan) about their size and size distribution at different stand-off distances. Correlation between particle sizes, their temperature and velocities were found out. Finally, the results from mathematical model were opposed to experimental results.

3 Results and Discussion

3.1 Numerical algorithm and results

The numerical treatment of coupled PDE systems that constitute an inviscid two-fluid/drift-flux model is a very challenging task. Most of the numerical algorithms published to date are based on a finite difference or finite volume discretization, while the use of finite elements is rather uncommon in this area of CFD research.

Our implementation of the new drift-flux model (1)–(3), (12)–(14) is based on a high-resolution finite element scheme which is applicable to unstructured meshes and implicit time-stepping schemes. A multidimensional generalization of Roe's approximate Riemann solver and an algebraic flux correction scheme of TVD type are constructed building on the methodology described in [21-23]. The design of the artificial viscosity operator, flux limiting and artificial implementation of the numerical boundary conditions are performed in terms of local characteristic variables. Particle-laden jets may give rise to low Mach number regions that co-exist with sonic points and local supersonic regions. The stiffness associated with the wide range of Mach numbers to be resolved calls for the use of an unconditionally stable implicit time discretization. Explicit schemes turn out rather inefficient, unless characteristic time stepping or local preconditioning is employed. The stationary counterpart of the above drift-flux model is solved using the fully implicit backward Euler method to match the solution to a steady-state. This pseudo-time-stepping scheme can be interpreted as an iterative solver, whereby the artificial time step serves as a variable under relaxation parameter.

The validation of the proposed drift-flux model in the context of thermal spraying processes is complicated by the lack of experimental data and reliable benchmarks for this class of multiphase flows. The numerical results for a prototypical 2D configuration are depicted in **Fig. 1**.

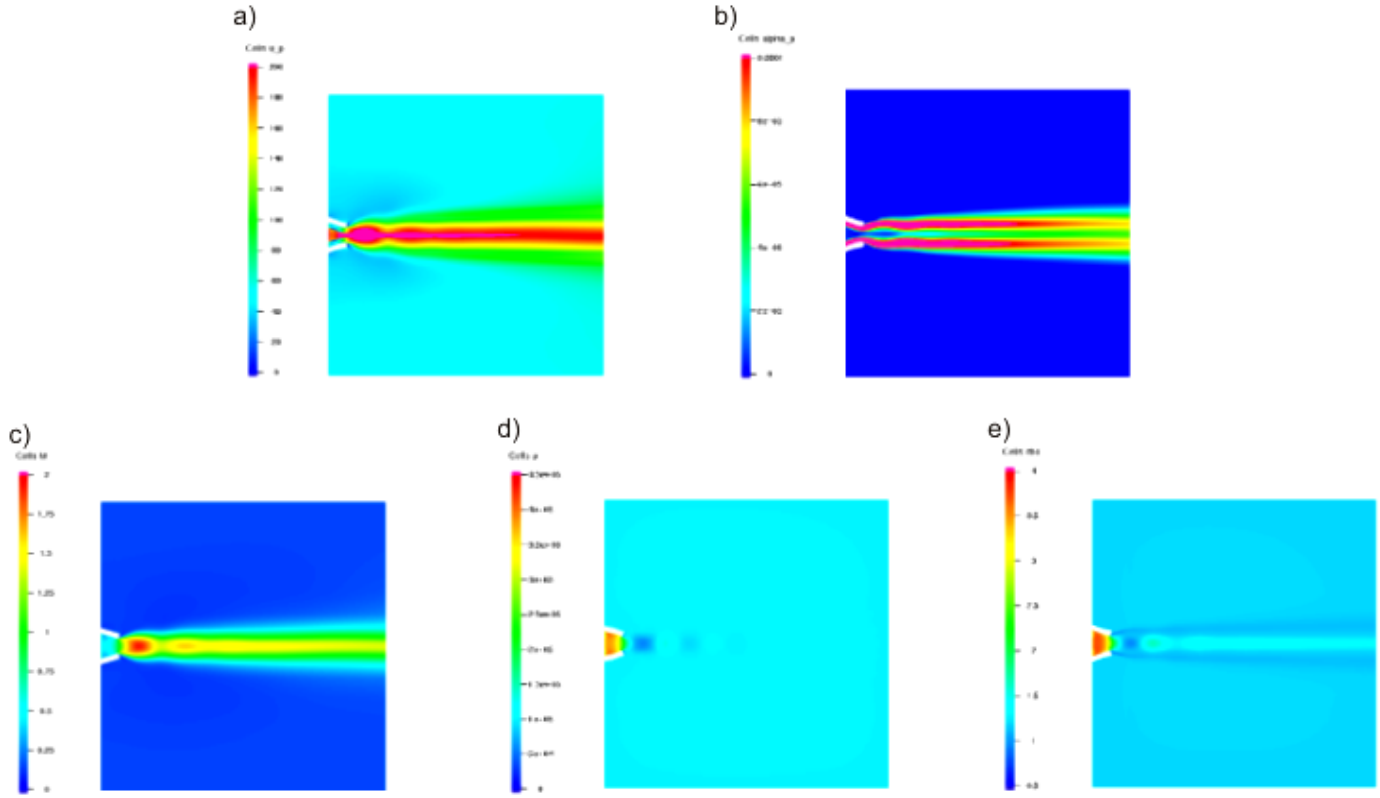

Fig. 1: Numerical results of a) particle velocity in m/s; b) volume fraction of particles in %; c) Mach number of the gas; d) gas pressure in Pa and e) gas density kg/m^3

A simplified nozzle is formed by two wires, which are modeled by solid walls and a gas-particle inlet in-between. Since no model of particle formation and atomization is available so far, the particles are injected through the boundary in the vicinity of the wires. The volume fraction of particles equals α_p=0.001 at the inlet. The dimensions of the computational domain are 0.8m×0.8m. Numerical solutions are computed on an unstructured triangular mesh with 48,785 nodes and a total of 390,280 unknowns.
The presented simulation results were computed using the supersonic boundary conditions:

$$M = M_g = 1.1, P_g = 0.2\text{MPa},$$
$$u_{2g} = u_2 = 0\text{m/s}, \rho_g = 2.3767\text{kg/m}^3$$

in the region between the wires and the slip condition on the wires. The slip conditions are implemented by projecting the residual and the solution on the tangent to the boundary. At the remaining boundaries, atmospheric conditions are prescribed for the incoming Riemann invariants. The density of the particles (nickel) is ρ_p=8908 kg/m^3 and the viscous drag is given by γ_D=1.26·10^6 kg/(s·m^3). At the post processing step, we assume that the particles move with the gas velocity if the volume fraction is less than 10^{-5}. This prevents division by zero and does not affect the computed solution.
It is observable that the velocity decreased along the spray jet. In a small distance after arc ignition the particle velocity was reduced approximately 30%. In this region the gas density and the Mach number of gas are too high. The particle velocity is also correlated with gas pressure. The higher the gas pressure is the faster the particles in the spray jet move. An axisymmetric particle flow can be detected. Hussary and Heberlein [7] came to the same conclusions by arc spraying at high voltages and low atomization gas pressures.

3.2 Spraying results

The results of particle velocities along the spray jet for both kinds of wires employed were shown in the **Fig. 2**. Particles generated from both wires exhibit the same behavior. The velocity of particles reduces up to a stand-off distance of 60 mm. With further increase of stand-off distance the velocities scale up to stay approximately constant up a stand-off distance of 80 mm. Owing to the high gas pressure of the spray jet at the outset area, which is verified from mathematical modeling (see **Fig. 1/d**), the generated particles are further atomized as a result of aerodynamic forces. Thereby turbulences, which are not modeled mathematically, are generated in this area, which in turn favor the particle atomization processes. These processes decelerated the particles associated with low particle velocities. The largest turbulences take place between at a 60 and 80 mm stand-off distance and no turbulences appear after stand-off distances of more than 80 mm. This explains the constant particle velocity levels after a stand-off distance of 80 mm as indicated also by the numerical results. After atomization particles with smaller sizes are produced, which move at the same gas pressure levels with higher velocities than the larger particles. However, the small particles can be more easily decelerated during flying, which explain the slight decrease of the Fe-based particles velocities at 150 mm stand-off distance.

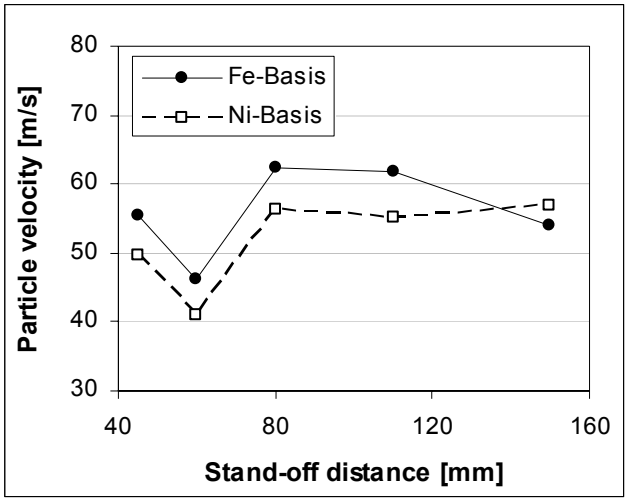

Fig. 2: Variation of particle velocity along the spray jet

By analyzing of arc jet with the high speed camera it can be established that after the first atomization of the melting bath large particles are produced. Along the spray jet they are fragmented in smaller particles. An axisymmetric breakup mechanism in the anode and a non-axisymmetric breakup mechanism in the cathode were detected [24]. This is not depicted by the mathematical model, since no modeling of particle atomization is performed. Thereby a further enhancement of the model is needed.

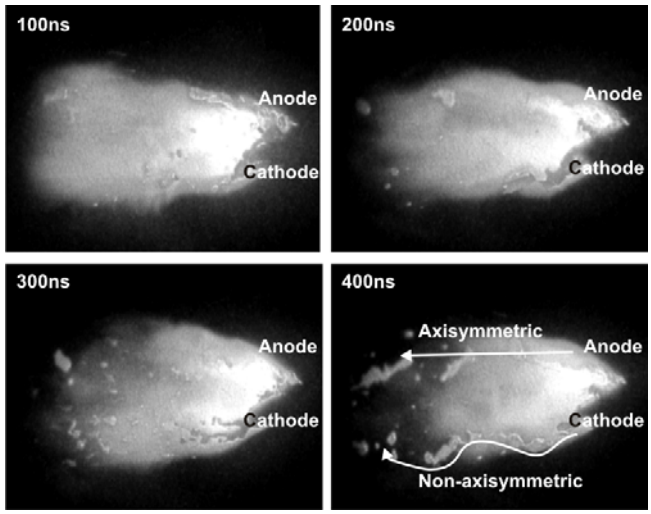

Fig. 3: High speed camera images of Fe-based wires at different sequences

Hussary and Heberlein [7] and Newbery et al [25] came to the same conclusion by arc spraying of metallic wires and by studying of steel wires spraying,

respectively. They explain this behavior with the aerodynamic forces and breakup mechanisms of molten bath.
It is noteworthy that the particles generated from Fe-based wires possess higher velocities than the particles generated from Ni-based wires. To explain this different behavior the particles generated from both wires during spraying were analyzed by means of SEM and light microscopy (**Fig. 4**).

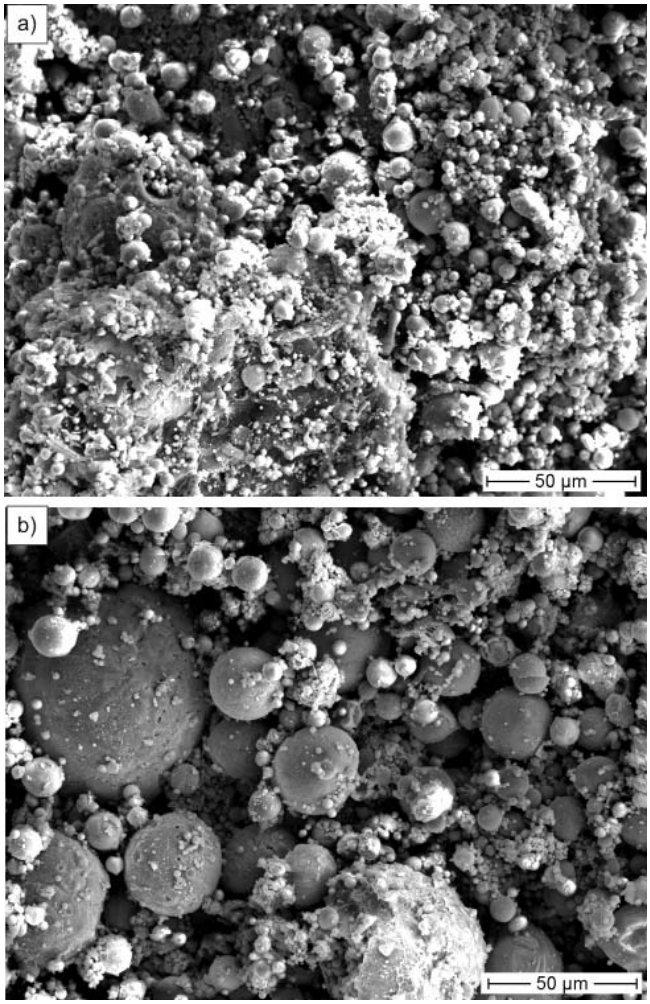

Fig. 4: Variation of particle size along the spray jet of a) Fe- and b) Ni-based particles

The Fe-based particles show a mean particle size of 6 µm, while Ni-based particles feature a mean particle size of 8.4 µm. It seems that the Fe-based particles have slightly smaller grain sizes that the Ni-based particles. This is confirmed from SEM-analyses. The different particle sizes are explained with different melting points of the wires. Ni-based wires have smaller melting points than the Fe-based wires [26], which are associated with a better atomization of Fe-based melting bath and smaller particle sizes. Further measurements by means of DTA (Differential Thermal Analysis) are needed to define the melting behavior of the cored wires used.
The particles` temperature shows a decrease of approximately 26 % with the stand-off distance independent from the kind of wires (**Fig. 5**). The atomization gas as well as the environment air impose a cooling effect on the accelerated particles. The smaller the particles are the larger the contact area with the gas is and thereby the higher the cooling effect is. Therefore the Ni-based particles with larger sizes feature higher temperatures than the Fe-based particles even though the Ni-based particles are accelerated with lower velocity.

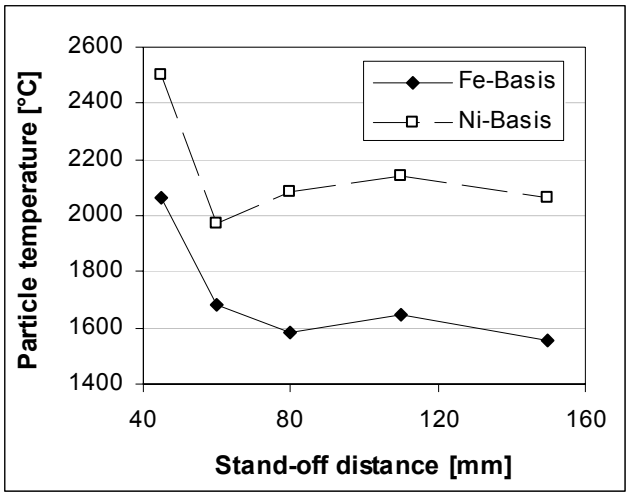

Fig. 5: Variation of particle temperature along the spray jet

4 Conclusions

A new mathematical model of Euler-Euler type was presented for the process of arc spraying. This model represents a generalization of the compressible Euler equations to particle-laden gas flows. Unlike the usual two-fluid model, the equations to be solved remain valid in particle-free regions. Promising results were obtained for a simplified 2D model problem. No turbulence, diffusion and wire/particle heating effects were considered so far. Further research is required to improve the robustness and efficiency of the numerical algorithm. Work is under way to impose characteristic boundary conditions in a weak sense and accelerate convergence to the steady-state using a nonlinear multigrid solver. Furthermore, an Euler-Lagrange model of particulate flow is to be implemented for validation purposes.
Experimental results show a deceleration of particles up to a stand-off distance of 60 mm due to the turbulences in this area. This is also associated with a further atomization of particles. An axisymmetric breakup mechanism was detected in the anode, while a non-axisymmetric breakup of the particles is characteristic for the cathode. It is also found that the higher the wires melting point is the less material melts and the smaller particles are generated. Due to the high surface area of smaller particle compared to the larger particles, the small particles cool down along the spray jet faster than the larger particles. Further analyses and measurements must be conducted at different pressure levels, voltages and electric currents to explain the melting behavior and

breakup mechanisms of cored wires during arc spraying.

5 Acknowledgement

The authors gratefully acknowledge the financial support of the DFG (German Science Foundation) within the Collaborative Research Centre SFB 708.

6 Literature

[1] Fr.-W. Bach, Th. Duda, Moderne Beschichtungsverfahren, Modern coating technologies, Wiley-VCH Verlag, Berlin, Germany, 2005.

[2] Wilden, J.; Wank, A.; Schreiber, F.: Wires for arc- and high velocity flame spraying – wire design, materials and coatings properties. Thermal Spray: Surface Engineering via Applied Research, C.C. Berndt, Ed., May 8-11, 2000 (Montréal, Québec, Canada), ASM International, Materials Park, OH, USA, 2000, pp. 609/17.

[3] M. Nakagawa, K. Shimoda, T. Tomoda, M. Koyama, Y. Ishikawa and T. Nakajima, Development of mass production technology of arc spraying for automotive engine aluminum alloy valve lifters, Thermal Spray Research and Applications, T. F. Bernecki, Ed., May 20-25, 1990 (Long Beach, California), ASM International, Materials Park, OH, USA, 1991, pp. 457/64.

[4] Lampmann, F.: Entwicklung einer Hybrid - beschichtungstechnologie zur Herstellung von Hochleistungs-Diesel-Pleuellagern. Dissertation TU Berlin, 2005.

[5] J. Wen, S. Wen, Aerodynamic behavior within the arc gap during arc spraying. Thermal Spray Industrial Applications, C.C. Berndt and S. Sampath, Ed., June 20-24, 1994 (Boston, MA), ASM International, Materials Park, OH, USA, 1994.

[6] T. Watanabe, X. Wang, E. Pfender, J. Heberlein, Correlations between electrode phenomena and coating properties in wire arc spraying. Thin Solid films 316 (1998), pp. 169/73.

[7] N. Hussary, J. Heberlein: Metal droplet formation mechanisms in the wire arc spraying process. Tagungsband 48. Internationales Wissenschaftliches Kolloquium, September 22-25, 2003 (Illmenau, Germany).

[8] Planche, M.P.; Liao, H.; Coddet, C.: Relations between in-flight particle characteristics and coating microstructure with a twin wire arc spray process and different working conditions. Surface and Coatings Technology 182 (2004), pp. 215/26.

[9] Schreiber, F.: Karbidische Werkstoffe zum Thermischen Spritzen. http://www.durmat.com/PDF-Files/d_Karbidische_Werkstoffe.pdf, DURUM-VERSCHLEISS-SCHUTZ GMBH, Willich.

[10] H. H. Tawfik, F. Zimmerman: Mathematical modeling of the gas and powder flow in HVOF systems, J. Thermal Spray Technol. 6 (1997), Issue 3, pp. 345/52.

[11] H. Hu, S.A. Argyropoulos: Mathematical modeling of solidification and melting: a review, Model. Simul. Mater. Sci. Eng. **4** (1996), Issue 4, pp. 371/96.

[12] S. Kamnis, S. Gu, N. Zeoli: Mathematical modeling of Inconel 718 particles in HVOF thermal spraying. Surface and Coatings Technology 202 (2008), Issue 12, pp. 2715/24.

[13] H. Städke: Gas dynamic Aspects of Two-Phase Flow, Wiley-VCH, 2006.

[14] D. Drew: Mathematical modeling of two-phase flow. Annu. Rev. Fluid Mech. 15 (1983), pp. 261/91.

[15] C. E. Brennen: Fundamentals of Multiphase Flows, Cambridge University Press, 2005.

[16] M. Pelanti, R. J. Leveque: High-Resolution finite volume methods for dusty gas jets and plumes, SIAM Journal of Science Computing 28 (2006), Issue 4, pp. 1335/60.

[17] T. Flatten, S. T. Munkejord: The approximate Riemann Solver of Roe applied to a Drift-Flux Two-Phase flow model. ESAIM 40 (2006), Issue 4, pp. 735/64.

[18] F. H. Harlow, A. A. Amsden: Numerical calculation of multiphase fluid flow. J. Comput. Phys. 17 (1975), pp. 19/52.

[19] T. Saito: Numerical analysis of dusty gas flows. J. Comput. Phys. 176 (2002), pp. 129/44.

[20] W. Tillmann, E. Vogli, M. Abdulgader: Influence of Atomisation Gas on the Particle Formation during Arc Spraying with Cored Wires. Thermal Spray 2007,: Global Coating Solutions, (Ed.) B.R. Marple, M.M. Hyland, Y.-C. Lau, C.-J. Li, R.S. Lima and G. Montavon, Published by ASM International, Materials Park, Ohio/USA, 2007, pp. 837/42.

[21] D. Kuzmin, M. Möller: Algebraic flux correction I. Scalar conservation laws. In: D. Kuzmin, R. L¨ohner and S. Turek (eds.) Flux-Corrected Transport: Principles, Algorithms, and Applications. Springer, 2005, pp. 155/206.

[22] D. Kuzmin, M. Möller: Algebraic flux correction II. Compressible Euler equations. In: D. Kuzmin, R. Löhner and S. Turek (eds.) Flux-Corrected Transport: Principles, Algorithms, and Applications. Springer, 2005, pp. 207/50.

[23] D. Kuzmin: Algebraic flux correction for finite element discretizations of coupled systems. In: E. Önate, M. Papadrakakis and B. Schrefler (eds.) Computational Methods for Coupled Problems in Science and Engineering II, CIMNE, Barcelona, 2007, pp. 653/56.

[24] N.A. Hussary, J.V.R. Heberlein: Effect of System Parameters on Metal Breakup and Particle Formation in the Wire Arc Spray Process. Journal of Thermal Spray Technology 16 (2007), Issue 1, pp. 140-52.

[25] A.P. Newbery, P.S. Grant, T.R.A. Neiser: The velocity and temperature of steel droplets during electric arc spraying. Surface and Coatings Technology 195 (2005), pp. 91/101.

[26] http://nt-systemloesungen.de/index.php?option=com_content&task=view&id=209&Itemid=171.